Performance Comparison of Joint Delay-Doppler Estimation Algorithms

Lorenz Mohr*, Michael Döbereiner†, Steffen Schieler*, Joerg Robert†,
Christian Schneider*†, Sebastian Semper*†, and Reiner S. Thomä*
* Technische Universität Ilmenau, Institute of Information Technology, Ilmenau, Germany
† Fraunhofer Institute for Integrated Circuits IIS, Ilmenau, Germany

***Abstract*— Integrated sensing and communications (ISAC), radar, and beamforming require real-time, high-resolution estimation algorithms to determine delay-Doppler values of specular paths within the wireless propagation channel. Our contribution is the measurement-based performance comparison of the delay-Doppler estimation between three different algorithms—comprising maximum likelihood (ML), convolutional neural network (CNN), and constant false alarm rate (CFAR) approaches. We apply these algorithms to publicly available channel data which includes two spherical targets with analytically describable delay-Doppler parameters. The comparison of the three algorithms features the target detection rate, root mean squared errors (RMSEs) of the delay-Doppler estimates, and a runtime analysis. Notably, all three algorithms demonstrate similar parameter estimation capabilities in bi-static scenarios, achieving target detection probabilities of up to 80 %. Conversely, forward and backward scattering conditions pose a problem to the estimation due to strong line-of-sight (LoS) contribution, reducing the corresponding detection probability down to 0 %.**

I. Introduction

Integrated sensing and communications (ISAC), radar, and beamforming are important research fields for the sixth-generation mobile communication standard. This technology necessitates a signal waveform that is capable of transmitting data and sensing the environment simultaneously [1], [2], [3]. As Braun [4] and Sturm [5] demonstrated in previous research activities, orthogonal frequency-division multiplexing (OFDM) fulfills this condition. They showed that such a signal facilitates delay, Doppler, and joint delay-Doppler estimation, while concurrently maintaining robust communication capabilities [6], [7]. In addition, ISAC requires high-precision and real-time capable delay-Doppler parameter estimation for sensing [8], [9], [10].

To perform such a parameter estimation, a multitude of algorithms exist. On one hand, there are discrete Fourier transformation (DFT)-based approaches. These algorithms estimate the propagation parameters by performing variations of a peak search in the delay-Doppler spectrum [7]. As the fast Fourier transformation (FFT) is a computationally efficient implementation of the DFT, these algorithms are well-suited for real-time applications at the cost of a finite resolution, limited by the bandwidths in time and frequency [11].

On the other hand, model-based algorithms estimate the target parameters by fitting an appropriate model to the received data. One example here is RIMAX, which performs delay-Doppler estimation based on an iterative maximum likelihood (ML) procedure [12]. Due to the analytical signal model, RIMAX is capable of separating closely spaced paths that are below the DFT resolution. Another example are physics-informed neural network (PINN)-based estimators. In [13], Schieler introduces such an algorithm, which is termed DeepEst within our work. This algorithm utilizes a convolutional neural network (CNN) structure in combination with a second-order gradient iteration to determine delay-Doppler values of specular propagation paths. However, the increased estimation accuracy of both RIMAX and DeepEst comes at the expense of a higher runtime compared to FFT-based approaches, resulting in diminished real-time capabilities [13].

Within this work, we present a comparison of the joint delay-Doppler estimation performance for three algorithms—RIMAX, DeepEst and ordered statistic constant false alarm rate (OS-CFAR)—in terms of target detection probability, root mean squared errors (RMSEs) of the estimates, and algorithm runtime. We perform this comparison utilizing channel measurements from a metrologically assessable setup in the sub-6-GHz frequency band including two moving spherical targets. Consequently, analytical ground truth values for the delay-Doppler propagation parameters of both spheres can be derived, enabling a direct comparison of the algorithms.

II. Measurement Data

A. Measurement Setup

Figure 1 depicts the measurement setup, which was originally introduced in [14]. Two metallic spheres (red circles) are mounted on a metal rod attached to a motor (+). Both TX and RX include horn antennas. The bistatic measurement angle δ spans between the TX, the turntable center, and the RX. This angle can be freely varied between 0° and 360°. Under these rotations, three different radar scenarios emerge from the setup—backward scattering ($\delta \approx 0°$), forward scattering ($\delta \approx 180°$), and bistatic scattering.

In addition, the measurement setup records Cartesian coordinates of TX, RX, and both sphere center points. Under the assumption that the diameter of the spheres is negligible, this setup enables a precise calculation of the theoretical propagation parameters—delay and Doppler—for the rotating targets. The equations for these calculations can be found in [14].

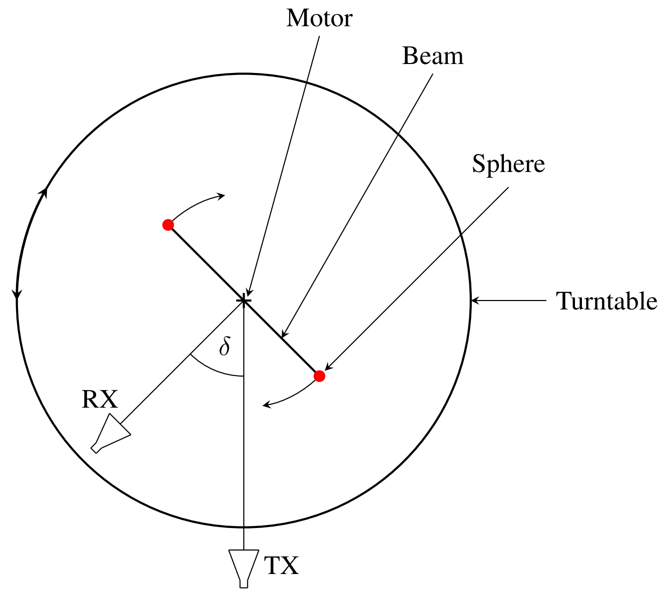

Figure 1: Bistatic Measurement Setup—Two metallic spheres (red) are mounted on a rotating beam. The bistatic measurement angle δ between transmitter (TX) and receiver (RX) creates either backward, forward, or bistatic scattering scenarios.

B. *Signal Model*

As introduced in [14], the measurement setup utilizes a multi-sinus waveform with Newman sequence phases to optimize the crest factor of the sensing signal. To perform delay-Doppler estimation of the spheres, we accumulate $L \in \mathbb{N}$ subsequent observations of the channel, each containing $K \in \mathbb{N}$ carriers, into a data frame.

By assuming an underlying sampling process of Δf in frequency and Δt in time, we describe the complex baseband channel transfer function $\mathbf{H} \in \mathbb{C}^{K \times L}$ by means of a parametric model as

$$\mathbf{H}_{k\ell} = \sum_{p=1}^{P} \gamma_p \cdot e^{-j2\pi k \tau_p \Delta f} \cdot e^{j2\pi \ell \alpha_p \Delta t} + \mathbf{N}_{k\ell}, \qquad (1)$$

where $\gamma_p \in \mathbb{C}$, τ_p, and α_p denote the p-th specular path in terms of weight, propagation delay, and Doppler-shift, respectively. The array $\mathbf{N} \in \mathbb{C}^{K \times L}$ is assumed to be drawn from an independent and identically distributed zero-mean circularly symmetric Gaussian process and models noisy observations of the channel. Since ground truth values for the path weights of the spheres are not available, we restrict this work to joint delay-Doppler parameter estimation.

III. Algorithms

The performance comparison of this work utilizes the estimation results of three algorithms, namely RIMAX [12], DeepEst [13], and a framework based on OS-CFAR [15].

A. *RIMAX*

The RIMAX algorithm is a ML-based estimator [12]. It estimates the paths within (1) though an iterative procedure, in which the parameters of all previously detected paths are refined using a gradient-based Gauss-Newton optimization. Subsequently, RIMAX validates the detected paths against the Cramér-Rao bound to assess the validity of the estimated parameters. If this test is passed, the contribution of the most recently detected path is subtracted from (1). The algorithm then continues the estimation on the residual data until the Cramér-Rao bound criterion is no longer satisfied.

B. *DeepEst*

In contrast, DeepEst is a PINN-based algorithm that utilizes a convolutional neural network to estimate the parameters of the specular paths within (1) [13]. The algorithm processes the data through three convolutional layers that perform channel upscaling, data downsampling, and channel downscaling, respectively. The output of the final convolutional layer is then passed to two linear layers, which estimate delay, Doppler, and path weight of the propagation paths. In addition, the algorithm includes a fourth convolutional stage followed by linear layers. This stage estimates the total number of paths P and discards unlikely paths identified in the third convolutional block.

C. *OS-CFAR*

We employ OS-CFAR in combination with selected pre- and post-processing techniques as a DFT-based baseline algorithm for comparison with RIMAX and DeepEst. Since the delay-Doppler spectrum exhibits pronounced sidelobes stemming from the limited aperture and process noise, conventional peak-based target detection results in numerous false alarms [11]. To mitigate this effect, the OS-CFAR algorithm estimates the noise level locally using ordered statistics [15], thereby reducing the number of false detections.

Although OS-CFAR successfully suppresses most false targets caused by side lobes and noise, strong static paths within the measurement setup still pose a problem for this algorithm. Specifically, when the bistatic measurement angle approaches $0°$ or $180°$, the line-of-sight (LoS) component dominates the received signal by several orders of magnitude, effectively shadowing the weaker reflections from the dynamic spheres [14]. To address this issue, we preprocess (1) using background subtraction and a two-dimensional Hamming window to remove static paths and attenuate sidelobes.

As OS-CFAR operates on a discrete delay-Doppler grid, the estimated parameters are inherently quantized. To improve estimation, we apply a two-dimensional quadratic interpolation in postprocessing to refine the parameters.

IV. Estimation Performance Comparison

The measurement data for this comparison is publicly available at [16]. Based on this data, we perform delay-Doppler estimation of the specular paths utilizing the hyperparameter settings listed in Table I. We then calculate the evaluation metrics—detection probability, estimation RMSEs, and runtime—by assigning the estimated paths to both spheres using their ground truth position information.

TABLE I: Hyperparameters

Hyperparameter	Value	Explanation
Measurement Data (Section II-B)		
K	1024	Number of subcarriers
L	100	Number of symbols
$\Delta\tau$	6.25 ns	Delay resolution
$\Delta\alpha$	156.25 Hz	Doppler resolution
RIMAX (Section III-A)		
P_{max}	25	Maximum number of paths
$n_{\text{grad}_{\text{max}}}$	50	Maximum number of gradient iterations
DeepEst (Section III-B)		
n_{grad}	10	Number of gradient iterations
OS-CFAR (Section III-C)		
m_{ref}	15	Reference window size in delay
n_{ref}	7	Reference window size in Doppler
r	79	Noise estimate index from (10) of [15]
α_{os}	11.39	Threshold scaling factor from (14) of [15]

A. Target Identification Boundary

The comparison between different algorithms depends on the choice of whether to identify an estimated specular path as a sphere reflection. We perform such an assignment if the estimated parameters are within half the delay-Doppler resolution (Table I) around the ground truth parameters of the sphere. In essence, this relaxed boundary accounts for estimation variance and measurement errors in the sphere positions, which translate to errors within the delay-Doppler ground truth [14].

Figure 2 illustrates the influence of the identification boundary on the target detection probability. Whereas the solid lines represent the default boundary of half the resolution, the dotted lines correspond to evaluations performed with a quarter-resolution boundary. As this boundary decreases, the target detection probability of each algorithm correspondingly diminishes. In essence, the default boundary ensures an acceptable target detection probability in bistatic scenarios while simultaneously maintaining a low number of false targets in both forward and backward scattering.

B. Comparison for One Bistatic Measurement Angle

We first compare the estimation results of RIMAX, DeepEst, and OS-CFAR for a bistatic observation angle of 20°. As this angle provides a bistatic scenario, the LoS is at least 30 dB weaker compared to backward and forward scattering, depicted by the red line in Figure 2. This LoS degradation arises from the horn antennas used in the measurement setup, described in Section II-A, which yield strong main and back lobes. In a bistatic scenario, the LoS of the TX antenna is positioned outside the main and back lobes of the RX antenna. Consequently, the LoS contribution to the data is reduced, allowing all three algorithms to achieve a detection probability of at least 60 % for the spheres.

Figure 3 depicts the temporal progression of the delay (top row) and Doppler (bottom row) estimation results for the three algorithms at the same bistatic observation angle.

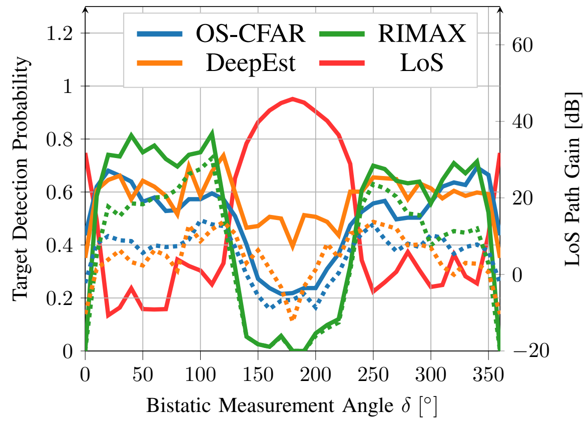

Figure 2: Detection Probability Compared to the LoS Strength—If the strength of the LoS decreases, the detection probability of each algorithm increases. While the solid lines depict this metric for the default identification boundary of half the delay-Doppler resolution, the dotted lines illustrate a quarter-resolution boundary.

In essence, DeepEst and OS-CFAR yield a target detection probability of approximately 60 %. Since RIMAX employs an iterative cancellation procedure, it achieves a detection probability exceeding 74 %.

Due to applied background subtraction, the estimation results of OS-CFAR and RIMAX do not incorporate any static paths. Consequently, Figure 3d and Figure 3f only depict a negligible number of detections that do not stem from the two spheres. DeepEst, on the other hand, does not include background subtraction and, therefore, detects mostly static paths. This accumulation around a Doppler-shift of 0 Hz causes delay estimations, where most detections do not align with the delay-Doppler ground truth of the spheres. In fact, the results of DeepEst demonstrate reflections with the measurement chamber wall and the motor housing, for example, at a delay of approximately 35 ns [14].

As illustrated in Figures 3d-3f, the Doppler estimations of each algorithm reveal the contribution of a linear frequency path emerging between 0.2 s and 0.4 s, and between 0.7 s and 0.9 s. This path originates from a reflection of the transmitted signal at the target emulator beam. As this beam rotates, the specular reflection center moves across its surface, resulting in the linear Doppler progression.

C. Comparison for All Bistatic Measurement Angles

As the bistatic measurement angle affects both the LoS strength and the absolute Doppler-shifts of the spheres, separating the spheres from the static paths becomes more challenging as this angle approaches 180°. Figure 2 depicts the dependency of the detection probability and the bistatic measurement angle for OS-CFAR (blue), RIMAX (green), and DeepEst (orange). The red line visualizes the strength of the LoS, which is inversely proportional to the target detection probability. In essence, the figure reveals that all

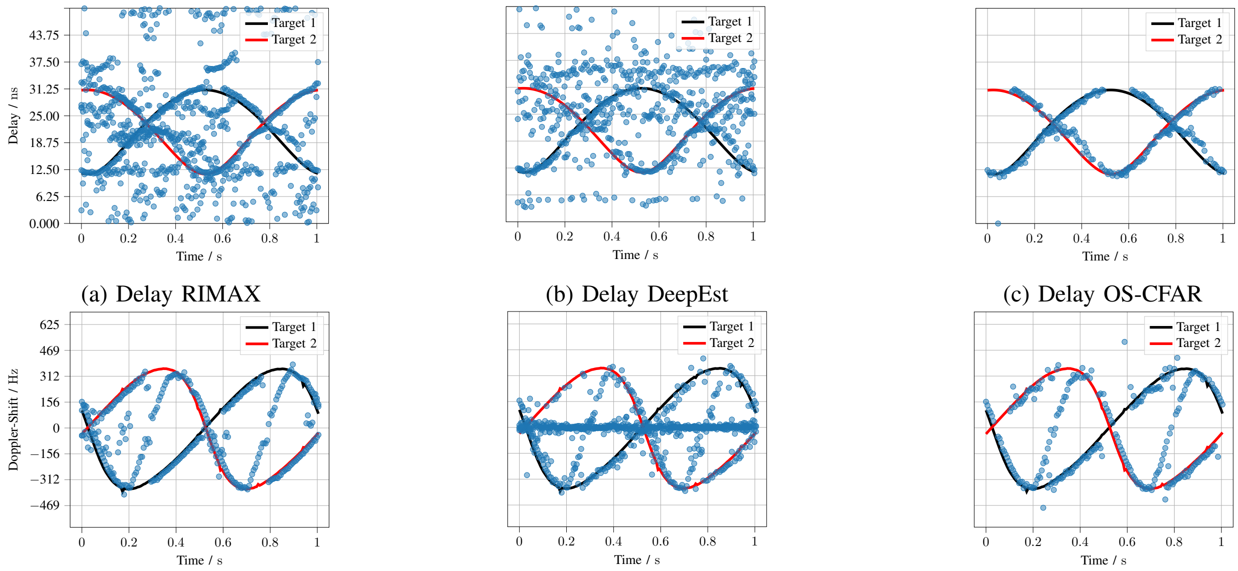

(a) Delay RIMAX (b) Delay DeepEst (c) Delay OS-CFAR

(d) Doppler RIMAX (e) Doppler DeepEst (f) Doppler OS-CFAR

Figure 3: Delay-Doppler Estimation Results for a Bistatic Observation Angle of $\delta = 20°$—The figures presents the estimation results for delay (first row) and Doppler-shifts (second row) of RIMAX (first column), DeepEst (second column), and OS-CFAR (third column). All plots include the results for one full rotation of the target emulator. DeepEst estimates a large number of static paths due to the missing background subtraction.

three algorithms share a similar dependency on the bistatic observation angle. Backward and forward scattering conditions pose a problem for sphere detections, yielding low probabilities down to $0\,\%$ for RIMAX. Conversely, bistatic scattering scenarios provide a higher number of true detections, with RIMAX being capable of estimating the two targets in more than $80\,\%$ of cases. The poor detection rates of RIMAX in backward and forward scattering are attributable to errors in the measurement hardware, which predominate in the delay-Doppler spectrum for strong LoS scenarios.

In addition, the availability of ground truth values enables the calculation of RMSEs for the delay-Doppler estimates. Figure 4 depicts the corresponding RMSEs, with the caveat that only successful sphere detections are included in the error calculation. It can be observed that the RMSEs for the three algorithms under consideration are comparable in both magnitude and progression across the full sweep of the bistatic observation angle. This finding aligns with the results presented in Figure 3, which indicate that the estimates closely follow the progression of the delay-Doppler ground truth for most time points. Notably, the maximum observed delay and Doppler RMSEs are $49\,\%$ and $36\,\%$ below the selected detection boundary of half the delay and Doppler resolution, demonstrating that this boundary does not limit the estimation accuracy of any of the algorithms.

However, Figure 4 exhibits anomalies when δ approaches $180°$. While the RMSEs of the proposed algorithm and RIMAX continue to decrease, those of DeepEst exhibit a maximum at this angle. This effect is caused by the lack of background subtraction in DeepEst. Consequently, DeepEst labels a significant number of static paths as sphere reflections. These falsely classified paths are further apart from the ground truth values, resulting in increased RMSEs.

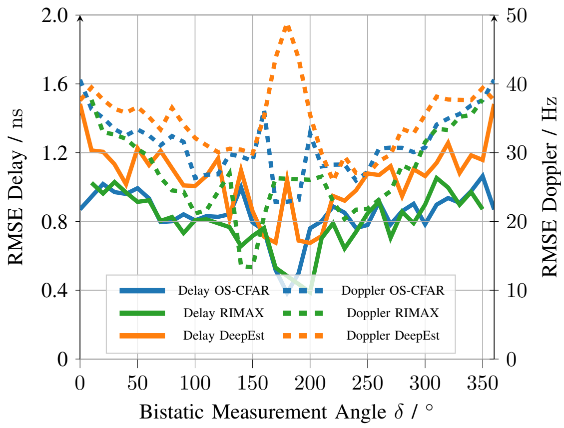

Figure 4: Delay and Doppler RMSEs—OS-CFAR (blue), RIMAX (green), and DeepEst (orange) exhibit similar RMSEs both in magnitude and progression. Due to an incorrect classification of static paths, the latter algorithm yields increased errors in forward scattering scenarios.

Finally, we perform a runtime analysis of the three algorithms. We compare their runtimes in terms of the mean execution time per radar frame, which is of size 1024×100. RIMAX requires on average $26.79\,$s to process a single frame. Conversely, DeepEst and OS-CFAR give an average of $2.02\,$s and $1.26\,$s per frame, respectively. Overall, our results indicate that the OS-CFAR-based framework is an accurate and comparably fast algorithm for delay-Doppler estimation, if the targets are not shadowed by stronger static paths.

V. Conclusion

Within our work, we compare the delay-Doppler estimation performance of three algorithms—approaches employing maximum likelihood (ML), convolutional neural network (CNN), and ordered statistic constant false alarm rate (OS-CFAR). For this estimation, we utilize publicly available channel data containing two moving spherical targets. We evaluate the three algorithms based on target detection probability, delay-Doppler root mean squared errors (RMSEs) of the target estimates, and algorithm runtime per frame.

As a result, the target detection probabilities demonstrate similar responses to a change in the magnitude of the line-of-sight (LoS). For LoS gains of approximately $0\,\mathrm{dB}$, the target detection probabilities of all algorithms exceed $60\,\%$. However, a $40\,\mathrm{dB}$ increase in this gain results in a significant absolute reduction of this probability by at least $30\,\%$. While achieving similar detection probabilities and RMSEs as the ML- and CNN-based approaches under weaker LoS conditions, the OS-CFAR estimator offers higher computational efficiency, with runtimes approximately $95\,\%$ and $33\,\%$ faster, respectively. However, owing to their high-resolution capabilities, the ML- and CNN-based algorithms outperform OS-CFAR when the targets are masked by stronger static paths.

To validate the results of our comparison, the presented algorithms should be applied to measurement data obtained outside a controlled environment. In such scenarios, which feature a higher number of targets as well as increased clutter and noise levels, ML- and CNN-based algorithms are expected to perform better due to their high-resolution capabilities and iterative cancellation procedures.

Acknowledgment

This work is sponsored by the BMFTR project 6G-ICAS4Mobility with Project No. 16KISK241.

References

[1] S. N. H. Shah, A. U. Khan, C. Schneider, and J. Robert, "SPYDER: QoS-Aware Radio Resource Allocation in Multiuser ISAC-Capable C-V2X Networks," *IEEE Open Journal of the Communications Society*, 2025. DOI: 10.1109/OJCOMS.2025.3558126

[2] Z. Wei et al., "Integrated Sensing and Communication Signals Toward 5G-A and 6G: A Survey," *IEEE Internet of Things Journal*, no. 13, 2023. DOI: 10.1109/JIOT.2023.3235618

[3] C. Sturm and W. Wiesbeck, "Waveform Design and Signal Processing Aspects for Fusion of Wireless Communications and Radar Sensing," *Proceedings of the IEEE*, no. 7, 2011. DOI: 10.1109/JPROC.2011.2131110

[4] K. M. Braun, C. Sturm, and F. K. Jondral, "Maximum likelihood speed and distance estimation for OFDM radar," in *Radar Conference, 2010 IEEE*, IEEE, 2010. DOI: 10.1109/RADAR.2010.5494616

[5] C. Sturm, T. Zwick, and W. Wiesbeck, "An OFDM System Concept for Joint Radar and Communications Operations," in *VTC Spring 2009 - IEEE 69th Vehicular Technology Conference*, IEEE, 2009. DOI: 10.1109/VETECS.2009.5073387

[6] Sturm, Christian and Braun, Martin and Zwick, Thomas and Wiesbeck, Werner, "A multiple target doppler estimation algorithm for OFDM based intelligent radar systems," in *The 7th European Radar Conference, Paris, France, 2010*, 2010.

[7] K. M. Braun, "OFDM Radar Algorithms in Mobile Communication Networks," Ph.D. dissertation, Karlsruher Institut für Technologie (KIT), 2014. DOI: 10.5445/IR/1000038892

[8] S. Semper, J. Naviliat, J. Gedschold, M. Döbereiner, S. Schieler, and R. S. Thomä, "Distributed Computing and Model-Based Estimation for Integrated Communications and Sensing: A Roadmap," *IEEE Open Journal of the Communications Society*, 2024. DOI: 10.1109/OJCOMS.2024.3467683

[9] A. Liu et al., "A Survey on Fundamental Limits of Integrated Sensing and Communication," *IEEE Communications Surveys & Tutorials*, no. 2, 2022. DOI: 10.1109/COMST.2022.3149272

[10] D. K. Pin Tan et al., "Integrated Sensing and Communication in 6G: Motivations, Use Cases, Requirements, Challenges and Future Directions," in *2021 1st IEEE International Online Symposium on Joint Communications & Sensing (JC&S)*, 2021. DOI: 10.1109/JCS52304.2021.9376324

[11] M. A. Richards, *Fundamentals of Radar Signal Processing*, Third edition. McGraw Hill, 2022, ISBN: 978-1260468717.

[12] A. Richter, "Estimation of Radio Channel Parameters," Dissertation, Technische Universität Ilmenau, 2005. [Online]. AVAILABLE: https://nbn-resolving.org/urn:nbn:de:gbv:ilm1-2005000111.

[13] S. Schieler, S. Semper, R. Faramarzahangari, M. Döbereiner, C. Schneider, and R. Thomä, "Grid-free harmonic retrieval and model order selection using convolutional neural networks," in *2024 18th European Conference on Antennas and Propagation (EuCAP)*, IEEE, 2024. DOI: 10.23919/eucap60739.2024.10501588

[14] A. Schwind et al., "Bi-static delay-Doppler reference for cooperative passive vehicle-to-X radar applications," *IET Microwaves, Antennas & Propagation*, no. 14, 2020. DOI: 10.1049/iet-map.2019.0991

[15] H. Rohling, "Radar CFAR Thresholding in Clutter and Multiple Target Situations," *IEEE Transactions on Aerospace and Electronic Systems*, no. 4, 1983. DOI: 10.1109/TAES.1983.309350

[16] A. Schwind and M. Döbereiner, *Sphere Carousel Dataset*, DOI to be provided at camera-ready version, 2025.